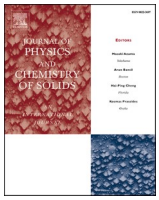
Journal of Physics and Chemistry of Solids 199 (2025) 112558



Contents lists available at ScienceDirect

Journal of Physics and Chemistry of Solids

journal homepage: www.elsevier.com/locate/jpcs



Technical note

Conduction band shift and interfacial charge transfer transition by adsorbed 4-teriary butyl pyridine analogues on TiO_2: A density functional theory study

Moyinoluwa O. Ashola, Richard K. Adeleke, Bolatito E. Olanipekun, Olusola O. James *

Department of Chemistry and Industrial Chemistry, Faculty of Pure & Applied Sciences, Kwara State University, Malete, Nigeria

ARTICLE INFO

Keywords:
Adsorption
Interfacial charge transfer
Conduction band edge
TiO_2

ABSTRACT

Additives are regular components in dye sensitized solar cell (DSSC) electrolyte preparations. 4-teriary butyl pyridine (4-TBP) is one of the most common additives in DSSC electrolytes. The role of 4-TBP at enhancing the open circuit voltage via negative shift of the conduction band edge of TiO_2 is widely recognised, however, its capability for interfacial charge transfer transition (ICTT) is unknown. In this contribution we use DFT to examine adsorption of 4-TBP and its analogues on TiO_2. The results show that 4-TBP is capable of ICTT in the UV region. Analogues bearing electron donating groups display ICTT in the visible region. While analogues bearing electron withdrawing groups may display no ICTT and cationic analogue displayed reversed ICTT. The results provide insights on the effect substituents on the negative shift of the conduction band edge of TiO_2. The results also revealed wider scope for selection of additives for enhancing the performance of DSSCs.

1. Introduction

Dye sensitized solar cell (DSSC) is one of emerging photovoltaic technologies that is expected to contribute significantly to the quest to increase the proportion of solar electricity in the global energy mix because of its low energy pay-back time [1,2]. DSSC is also appealing because of its higher low light efficiency than silicon based solar cells and easy integration into building as windows, wall etc [3]. In order to further make DSSC attractive for wider applications such solar fuels production, internet of things [4], etc., a number of strategies are being explored to improve conversion efficiency of DSSC [5]. The power conversion efficiency is directly related to the open circuit voltage (V_{oc}) and the short circuit current (J_{sc}) [6].

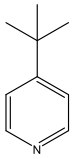
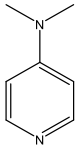
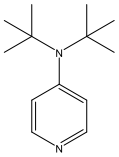
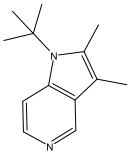
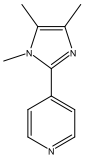
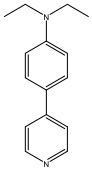
The current product by a DSSC is a function of light harvest, electron injection and charge collection efficiencies [7]. The value of J_{sc} depend partly on the individual and interfacial processes between the four DSSC components (the semiconductor, TiO_2; the sensitizer, dye; the redox mediator, e.g iodide/triiodide; and the counter electrode) [8,9]. However, the value of V_{oc}, is determined by the difference between the semiconductor conduction band and the redox potential of the redox mediator. Pursuits of increase of V_{oc} are through reduction of voltage losses from electron injection driving force, recombination processes and regeneration energy of the oxidised dye [10,11]. Iodide/triiodide redox couple is one of the early effective redox mediators that is popularly used in DSSC devices. Hence, V_{oc} values of early DSSC devices are limited by the redox potential of redox potential of iodide/triiodide redox couple. Larger V_{oc} values were obtained when iodide/triiodide redox couple is replaced by cobalt complexes and later copper complexes redox couples via reduction of regeneration energy [12].

Another strategy being employed for improving the conversion efficiency of DSSCs is addition of Lewis bases to the redox mediator solution. The inclusion of Lewis bases in DSSCs redox electrolytes is primarily to impact surface passivation of the TiO_2 via adsorption on coordinatively unsaturated surface TiO_2 sites. The surface passivation suppresses unwanted recombination between injected electron into TiO_2 and redox mediator in the electrolyte [13–15]. For this purpose, 4-*tert*-butylpyridine (TBP) became a ubiquitous additive in electrolytes of because of its pyridine nitrogen and hydrophobic tail. Moreover, it has also been shown that TBP adsorption on TiO_2 raises the energy level of conduction band of TiO_2 [16]. The elevation of TiO_2 conduction band energy level increases the V_{oc} at the expense of reduced electron injection driving force. Another commonly employed electrolyte additive in DSSC is lithium ion (Li^+). Contrary to TBP adsorption of Li^+ shifts down the conduction band edge of TiO_2 [17,18]. Accumulation of Li^+ on TiO_2

* Corresponding author.
E-mail address: olusola.james@kwasu.edu.ng (O.O. James).

https://doi.org/10.1016/j.jpcs.2025.112558
Received 30 October 2024; Received in revised form 17 December 2024; Accepted 5 January 2025
Available online 6 January 2025
0022-3697/© 2025 Elsevier Ltd. All rights are reserved, including those for text and data mining, AI training, and similar technologies.

Table 1
4-TBP analogues with strong electron donating para substituents.

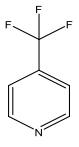
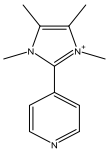
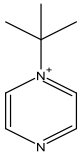
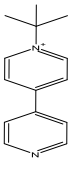
					
4-(*tert*-butyl) Pyridine (4-TBP)	4-(N,N-dimethyl amine) pyridine	4-(N,N-di-*tert*-butylamine) pyridine	1-(*tert*-butyl)-2,3-dimethyl-1H-pyrrolo [3,2-c] pyridine	4-(1,4,5-trimethyl-1H-imidazole-2-yl)pyridine	4-(N,N-diethyl aniline) -4-pyridine
A	B	C	D	E	F

surface had been shown to passivate TiO_2 surface, stabilize electrons in the TiO_2 and also induces Stark effect the sensitizers [19].

Although, the combine inclusion of Li^+ and TBP in an electrolyte results in improve performance TiO_2-based DSSCs, the V_{oc} is kept at value because the effect of TBP on the conduction band edge of TiO_2 is cancelled out by the of Li^+. But V_{oc} increase through elevation of the conduction band edge of TiO_2 is still desirable. Moreover, it has been shown recently that TiO_2 interaction with pyridine bearing strong electron donating groups can result interfacial charge transfer transition (ICTT) in the visible region [20]. By extrapolation, it implies that TBP and other Lewis bases so far used as additives in DSSC, do not produce ICTT in the visible. Conversely, use of additives that are capable of ICTT in the visible can be exploited in synergy with a sensitizer for panchromatic absorption as a DDSC photoanode. The effect of adsorbed organic additive on TiO_2 provide is one of the strategies for TiO_2 band edge engineering [21,22]. Moreover, additive-TiO_2 complexes that are capable ICTT in the visible region had been shown to exhibit enhanced photocatalytic activities [23]. Therefore insights on additive structure for achieving ICTT will be beneficial for rational design of additive-TiO_2 for hydrogen production [24] and photocatalysis in general [25].

In this contribution we use DFT calculations to gain insights about ICTT involving TiO_2. We choose TBP as reference because its wide usage in DSSC electrolytes and recently its electron donating analogues had been shown to displayed ICTT in the visible region. Typical I^-/I_3^- based DSSC electrolytes consist: iodide salt, iodine, TBP, dissolved in acetonitrile (or other low viscosity aprotic polar solvent). The cation of the iodide salt is usually are Li^+ and or 1,3-dialkylimidazolium. Cationic TBP analogues that posses combined properties of TBP and imidazolium (or other organic cations) can serve the dual-function TBP and Li^+ or 1,3-dialkylimidazolium thereby leading to a simplified DSSC electrolyte recipe. Such cationic TBP analogues will constitute electron withdrawing counterpart to the aforementioned electron donating TBP analogues. But there is yet any systematic study on ICTT of electron withdrawing TBP analogues on TiO_2. Therefore, it is desirable to interrogate this information gap by examining adsorption interaction, electronic, and optical properties of the TiO_2–TBP analogues (TiO_2-pyd) complexes and comment on their implications for DSSC applications.

Table 2
4-TBP analogues with strong electron withdrawing para substituents.

			
4-(trifluoromethyl) pyridine	4-(1,3,4,5-tetramethyl imidazolium)-2-pyridine	1-(*tert*-butyl) pyrazin-1-ium	1-(*tert*-butyl)-[4,4′-bipyridin]-1-ium
G	H	I	J

2. Materials and methods

All computations were performed using the Orca 4.2.1 quantum chemistry package [26]. For the adsorption studies, a TiO_2 cluster [$Ti_{10}O_{19}(OH)_2$] was constructed using Avogadro software [27]. Density functional theory (DFT) and time-dependent DFT (TD-DFT) calculations were carried out on the model TiO_2 cluster(total charge = 0). O3LYP functional and def2-SVP def2/J basis set was found to give HOMO and LUMO levels that is closest to the conduction band edge and band gap of bulk TiO_2 anatase. The same functional and basis set was used for all optimization, vibrational and optical calculations. The TiO_2–pyd complexes calculations were carried out according the protocol reported by Fujisawa et al. [28]. For optimization of the complexes, optimised coordinates of the atoms of the TiO_2 cluster were frozen, while all atoms of the pyridine derivatives were relaxed. The frequency calculations of the organic and TiO_2-organic complex were performed in acetonitrile using the SMD solvation model. The model uses the CPCM algorithm with different radii to create the cavity and calculates a different non-electrostatic contribution, the cavity-dispersion-solvent structure. No symmetry limitations were imposed during the calculations. TD-DFT calculation were performed using the optimised coordinate and the orbitals energies profile were extracted from the output file using GaussSum 3.0 software [29].

3. Results and discussion

There is no general consensus on the minimum cluster size to sufficiently model the bulk properties of $(TiO_2)_n$, $n = \infty$. The guiding principle is striking a rational balance between accuracy and computational costs [30]. Although, one study claimed that a cluster size $n = 6$ is sufficient to reproduce the band gap of bulk TiO_2 [31], we started with cluster size $n = 8$, and explored for the functional and basis set that reproduce the band gap of bulk TiO_2. We tested GGA (BP86) and hybrid GGAs (B3LYP, PBE0, B3PW91 & O3LYP) functionals. O3LYP gave LUMO and HOMO energy level 4.032 and 7.692 which give a band gap close to that of anatase TiO_2(supplementary information). It also present LUMO energy level that is close the conduction band edge of anatase TiO_2.There is no accuracy benefit in using basis set def2-TZVP def2/J over def2-SVP def2/J. The LUMO and HOMO of the model cluster is similar to that reported by Fujisawa et al. with $n = 34$ cluster size [20,32,33]. Although B3LYP is widely in many DFT calculations, we found O3LYP more suited in this study. There are report that show that O3LYP compares fairly well or better in some cases than B3LYP at estimation properties of organic molecules. Hence, we elect to use O3LYP functional and def2-SVP def2/J basis set for all the calculations. We further test robustness of the cluster model and calculation parameters by applying it to reproduced the reported interfacial charge transfer transition of adsorbed anthroic acid on TiO_2 [28]. The result obtained for $(TiO_2)_n$, $n = 1$ is less convincing, but that $(TiO_2)_n$, $n = 10$ clearly demonstrate the ICTT (supporting information).

TBP is a standard electrolyte additive in many DSSC device fabrications. TBP as a Lewis base, interact with Lewis acid site on TiO_2

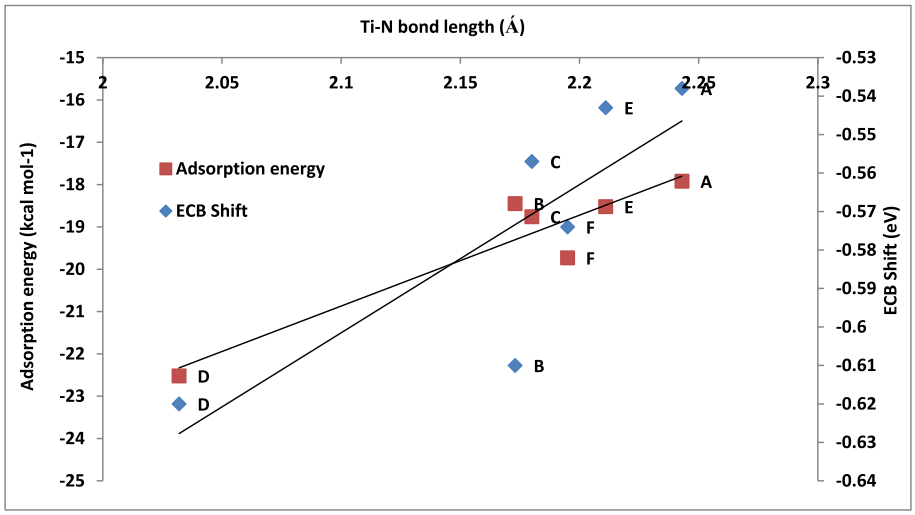


Fig. 1. Adsorption energy and conduction band edge shift vs Ti–N bond length of TBP analogues bearing strong electron donor.

surface. The hydrophobic tertiary butyl tail point outwards to provide passivation cover which physically blocked access of oxidised species of redox mediators to the TiO_2 surface. The adsorptive interaction caused a negative shift of the conduction band edge of TiO_2. The shift was attributed to the dipole moment component of TBP component normal to the TiO_2 surface plane [34]. The elevation of the conduction band edge enhanced the open-circuit photovoltage (V_{oc}) but at the expense of decreased short-circuit photocurrent density (J_{sc}). To further interrogates the TiO_2-TBP interaction via Ti–N coordinate bond, we scout for structurally similar pyridine derivatives with bulky strong electron donating and bulky strong electron accepting substituents at the para position. The pyridine derivatives are shown in Tables 1 and 2.

The TiO_2−Pyridine derivatives complexes were optimised. For the geometry optimization all the titanium and oxygen atoms in the model TiO_2 cluster were frozen, while all the other atoms were relaxed. The Ti–N bond lengths in the optimised complexes were obtained by visualising the orca output using Avogadro software. The adsorption energies of the pyridine derivatives on TiO_2 where determined from frequency calculations. As shown in Fig. 1, both the adsorption strength of the pyridine derivatives and their effect on the extent of the negative shift of the conduction band edge of TiO_2 varies inversely as the Ti–N bond lengths. It implies that as the electron-donating ability of the pyridine derivatives increases the Ti–N bond becomes stronger. This is consistent with results obtained for similar calculations on adsorption heterocyclic molecules on TiO_2. It is also in line with the report of Fijuwara et al. [20] on the substituent effects on the adsorption density of pyridine molecules. The extent of negative shift of the conduction band edge of TiO_2 increases with increase in the electron-donating ability of the substituents, although the effect of the electron donor groups relative that of tertiary butyl may be considered marginal. It is noteworthy that D stands out among the analogues.

The analogues bearing electron donating groups have shorter Ti–N bond length compared to TBP. Conversely, the analogues bearing electron withdrawing groups have longer Ti–N bond lengths compared to TBP. Also, the extent of negative shift of the conduction band edge of TiO_2 by the analogues bearing electron withdrawing groups are slightly lower compared to that of TBP except for I. In the outlier, 'I', the positive charge is situated within the pyrazine ring which exerts mesomeric and inductive electron withdrawing effects on the lone pair of electrons on the second pyrazine nitrogen [35]. This weakens the basicity of the nitrogen for sigma electron donation into vacant orbitals of surface TiO_2. It is interesting to note that despite disparity large in the Ti–N bond lengths of 'A'and 'G' vs 'I', their adsorption energies are within a close range. This suggests that the nature of interaction of 'A' and 'G' with TiO_2 is similar and it is disparate from that of 'I' with TiO_2. Likewise, 'H' and 'J' shares similarities in terms of nature of interaction with TiO_2, which

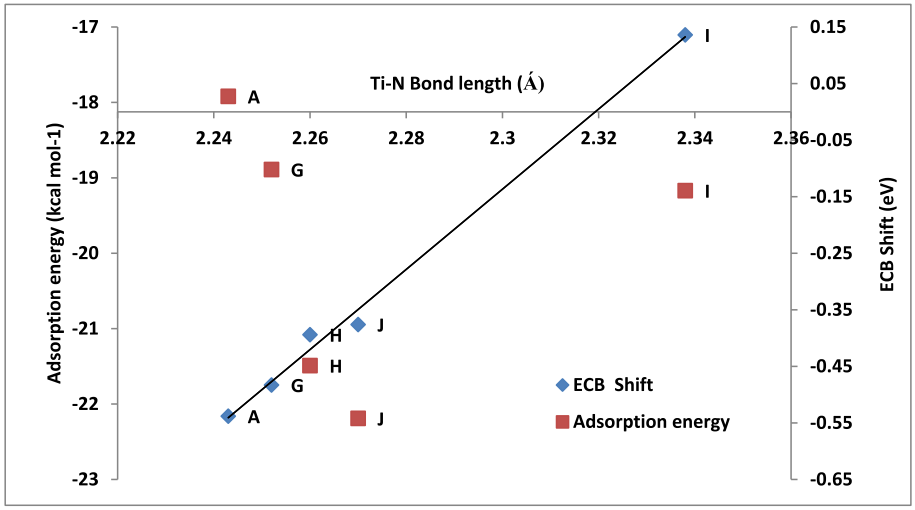


Fig. 2. Adsorption energy and conduction band edge shift vs Ti–N bond length of TBP analogues bearing strong electron withdrawing groups.

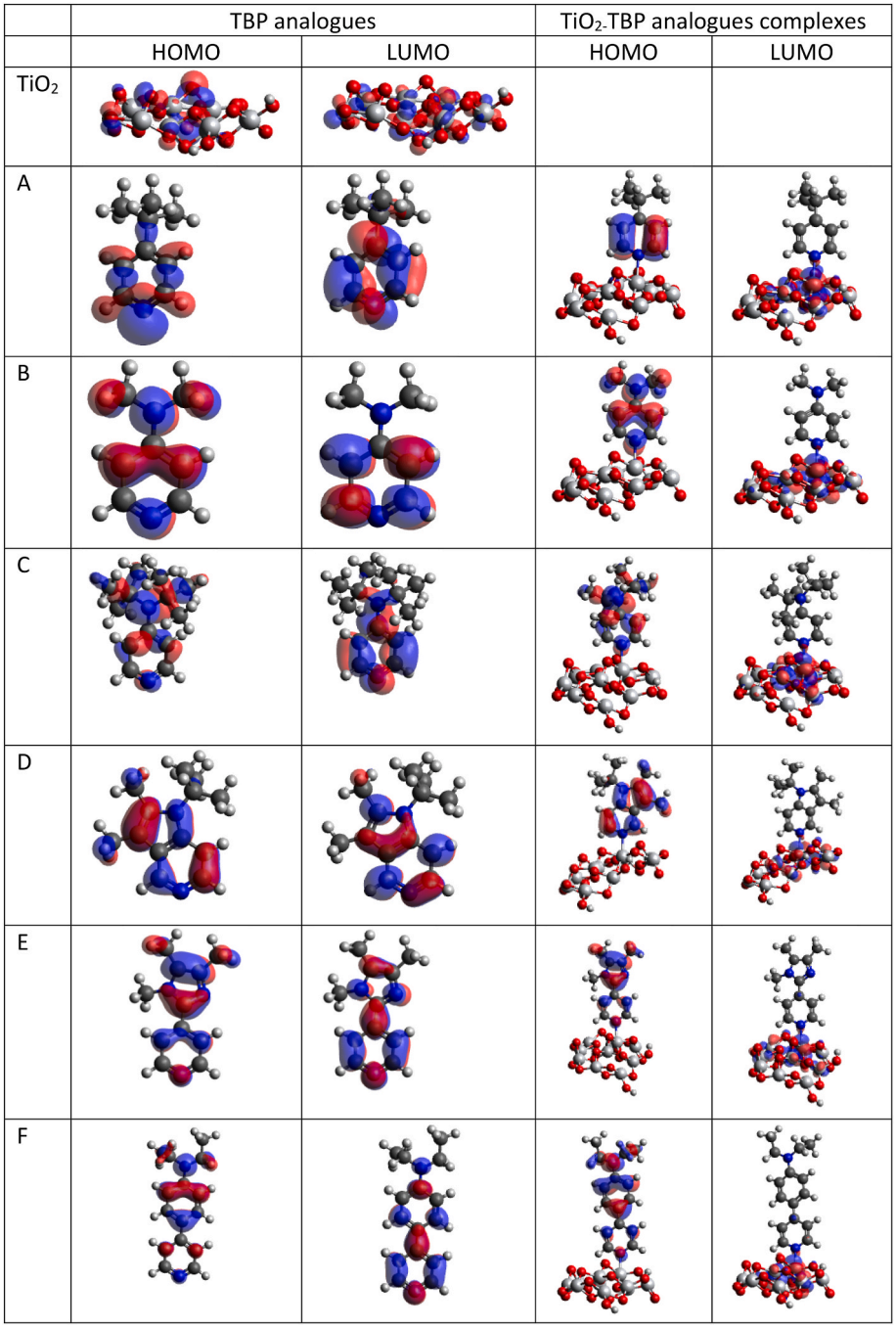


Fig. 3. Frontier orbitals of TiO2, TBP and TBP analogues bearing electron donating groups.

combined fractions of the nature of interactions of 'A' and 'I'.

To gain more insights on the interactions of TBP analogues with the model TiO_2 cluster, we examined their frontier orbitals and that of their complexes with the TiO_2 cluster (Fig. 3). As shown in Fig. 3, the HOMO of TBP and the analogues except D shows a non-bonding lone pair orbital protruding on the nitrogen outside the aromatic ring. The electron donating groups of the TBP analogues also consist of another non-bonding lone pair orbital(s). These lone pairs inductively or conjugatively increases the electron density in the aromatic ring, destabilize and raise the energy level of the occupied pie orbitals of the analogues. The HOMOs A, B & C indicated high density of the non-bonding lone pair orbitals, but it contracted in E and F and virtually absent in D. This may be explained by the extent of conjugation of the non-bonding lone pair orbital with the aromatic ring. The lone pair orbital of the pyridine nitrogen in D is strongly conjugated and delocalised over the whole molecules. As shown in Fig. 3, upon adsorption the HOMO of TiO_2-TBP complex is localised in TBP and the LUMO is localised in the TiO_2 cluster, clearly indicating that HOMO-LUMO transition is an interface charge transfer transition (ICTT). The same is depicted for the TiO_2 complexes of the TBP analogues. Thus, it can be inferred that barring steric restriction both the localised and delocalised non-bonding lone pair orbitals can efficiently coordinate with vacant orbitals on the surface of the TiO_2 cluster.

The orbital diagrams in Fig. 3 do not indicate the region the ICTT will be observed. But according to Fujisawa et al., the conditions for creating ICTTs in the visible region are: (i) the HOMOs of the organic component should be located within the band gap of TiO_2; (ii) overlap between the HOMOs of the organic component and the conduction band of TiO_2 (or

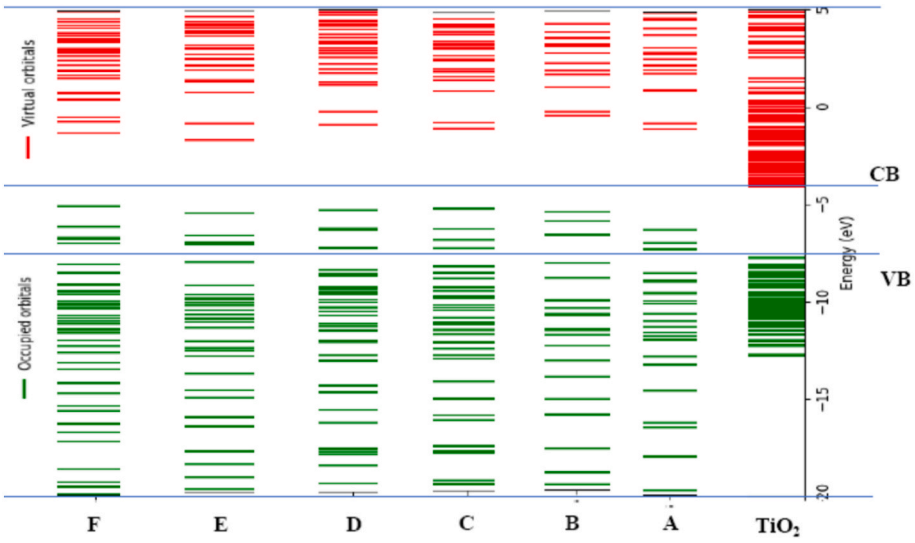


Fig. 4. Occupied and unoccupied orbitals energies profiles of TiO_2, TBP and TBP analogues bearing electron donating groups.

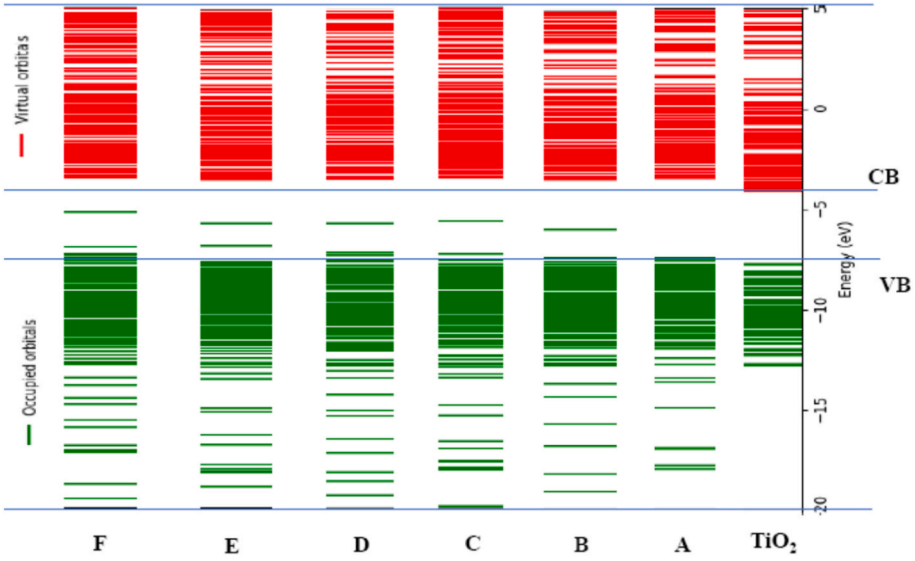


Fig. 5. Occupied and unoccupied orbitals energies profiles of adsorbed TBP and TBP analogues bearing electron donating groups on TiO_2 cluster.

any inorganic component). Fig. 4 shows the HOMOs and LUMOs energies of TBP and the analogues relative to that of the TiO_2 cluster. The figure shows that the top HOMOs of TBP and the analogues are within the band gap of TiO_2, satisfying the first condition. As discussed earlier, replacing the tertiary butyl in TBP with stronger electron donating group increases the electron density in the aromatic ring, destabilized and push the HOMOs upwards in the TBP analogues. This account for higher energies of the HOMOs of the analogues relative to that TBP. Also, the stronger electron donating groups alters the configuration and electron densities on the non-bonding lone pair orbital of the pyridine nitrogen. This will influence coordination on the TiO_2 surface.

The degree of overlap between the HOMOs of TBP or the analogues and the conduction band of the TiO_2 cluster will depend on the proximity of the respective pairs. Elevated HOMOs of the analogues are closer to the conduction band of the TiO_2 cluster than that of TBP. Thus, the degree of overlap of the HOMOs – CB (TiO_2) in the TiO_2-analogues complexes are expected to stronger than in the TiO_2-TBP complex. The resulting orbitals energies profiles of the complexes are shown in Fig. 5. The profiles show raised conduction and valence band edges in TiO_2-TBP complexes relative to that of the TiO_2 cluster. The shift of the conduction band edge is higher than the valence band edge shift. Thus, resulting in increase in the band gap of the TiO_2-TBP complex compared to bare TiO_2, and restricting the ICTT here to the UV region. In the profiles of the TiO_2-analogues complexes, the conduction band edge shifts are nearly the same as in the TiO_2-TBP complex, however, the conduction band edge shifts are higher and even show one or more intermediate occupied level within the band gap. The gap between the intermediate levels and the raised conduction band are in the visible region. Hence, transitions from the intermediate occupied levels of the TiO_2-analogues complexes to the raised conduction band will result in ICTT in the visible region. Therefore, the second condition for ICTT in the visible region is not as simple as stated by Fujisawa et al., the overlap between the HOMOs of the organic component and the conduction band of TiO_2 resulted in creation of intermediate occupied level within the band gap of the TiO_2-organic complex.

Fig. 6 shows the frontier orbitals of the TBP analogues bearing electron withdrawing groups. As observed for the analogues with electron donating groups, the non-bonding lone pair electron on the nitrogen in the pyridine ring. In contrast to the electron donating, the electron withdrawing group inductively and or conjugatively decreases

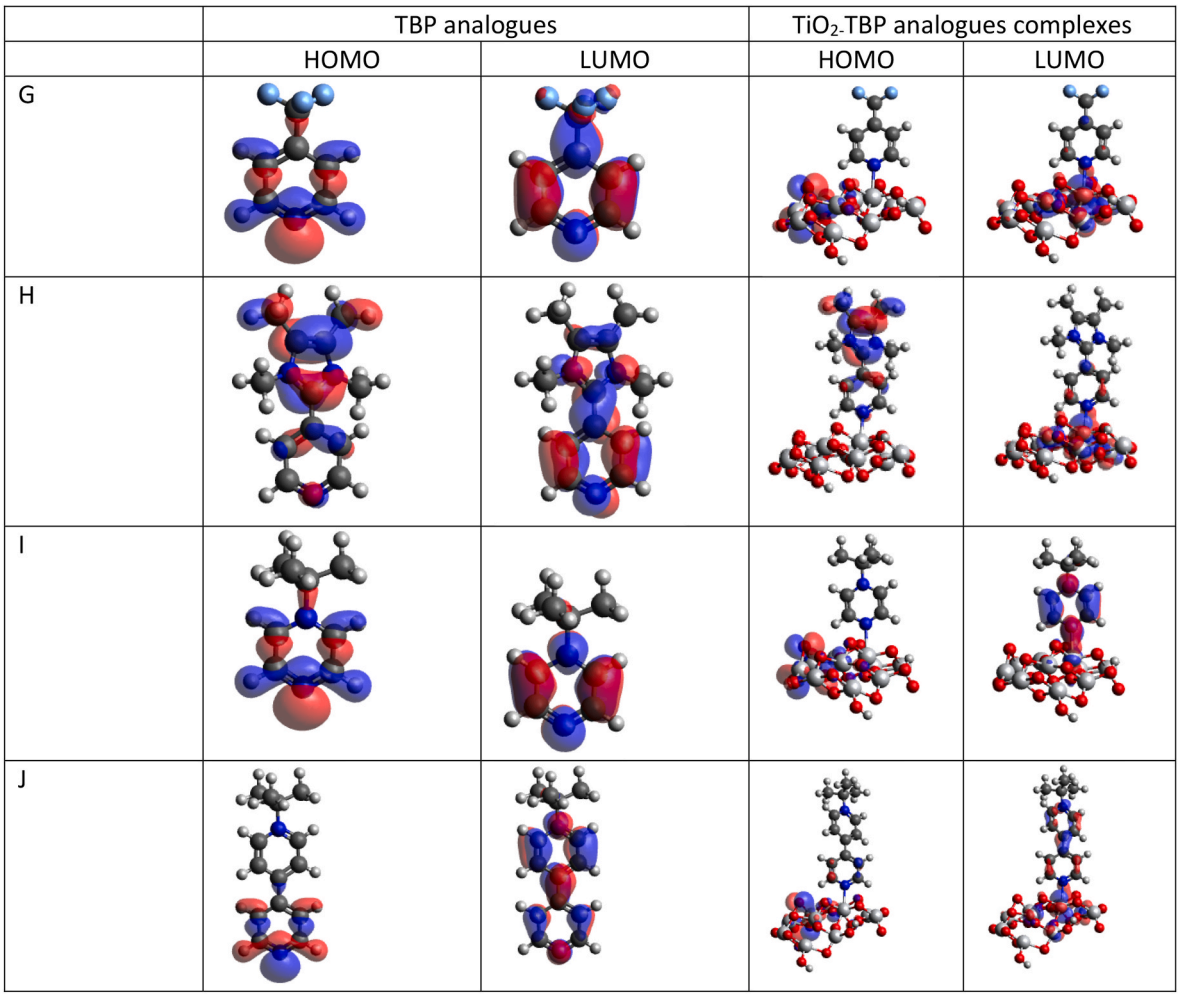


Fig. 6. Frontier orbitals of $TiO_2$and TBP analogues bearing electron withdrawing groups.

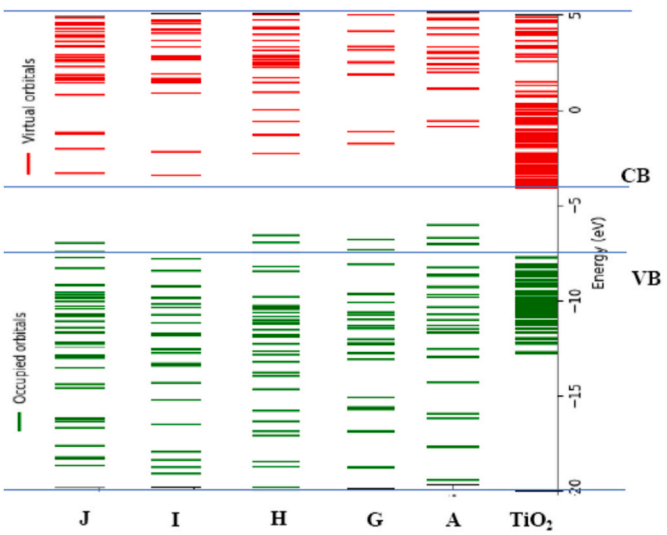


Fig. 7. Occupied and unoccupied orbitals energies profiles of TiO_2, TBP and TBP analogues bearing electron withdrawing groups.

the electron densities of non-bonding lone pair orbital. This reduces the electron densities for coordination with vacant orbitals on the surface of the TiO_2 cluster. It is also consistent with the longer Ti–N bond lengths and the decreased extent of shift of the TiO_2 conduction band edge obtained for the complexes of the electron withdrawing analogues relative to those of the electron donating ones. As state earlier from Fig. 2, H and J have adsorption energy and Ti–N bond lengths that are comparable to those obtained for some electron donating analogues in spite of the reduce electron density on the lone pair orbital for coordination with TiO_2. This may be attributed to contribution from the occupied pie orbitals of these analogues to the coordination with TiO_2. This is especially corroborated by high density of pie orbital contribution to the HOMO of H. The HOMO and LUMO of G resides in the TiO_2, suggesting no ICTT in G. however, the HOMO of H resides in the imidazolium ring while the LUMO is localised in the TiO_2 cluster, indicating ICTT can occur in H. The HOMO of J is localised in the TiO_2 while its LUMO is delocalised between TiO_2 cluster and the analogue. This depicts a transition toward reverse ICCT. And in the case of I, a clear-cut reverse ICTT can be invoked because the HOMO is localised in the TiO_2 cluster while the LUMO is localised in the cationic molecule.

As shown in Fig. 7, the HOMOs and the LUMOs of the electron withdrawing group bearing analogues are more stabilised relative to that of TBP. Their HOMOs and the LUMOs energy levels are deeper compared to that of TBP. The HOMOs are far from TiO_2 conduction band edge and thus preclude them from requirement of being situated within the band gap of TiO_2. This implies they are unable to satisfy the conditions for creating ICTT in the visible region. It is worth noting that the LUMO levels of I and J, are sufficiently close and can efficiently overlap with the conduction band edge of the TiO_2 cluster. So, when the LUMO level of an adsorbate is close or deeper than the conduction band edge of TiO_2 (or inorganic semiconductor) overlap is likely to take place. This

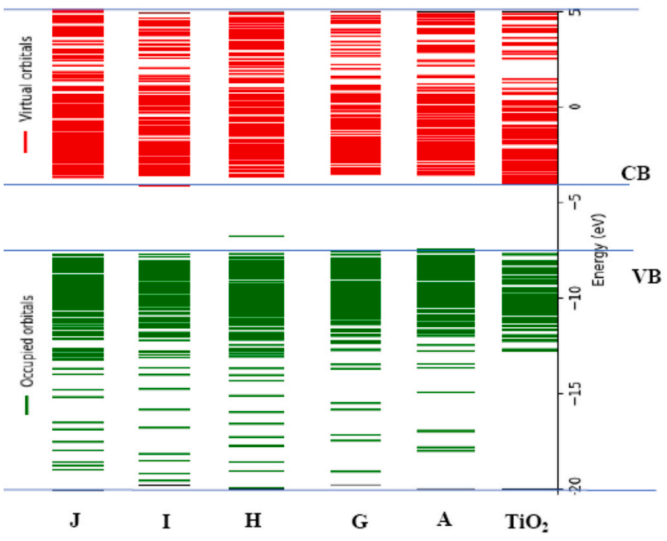


Fig. 8. Occupied and unoccupied orbitals energies profiles of adsorbed TBP and TBP analogues bearing electron withdrawing groups on TiO_2 cluster.

overlap accounts for the observed reversed ICTT for I in Fig. 6. Instead of intermediate occupied level with the band gap, an intermediate unoccupied level is created below the conduction band edge in the TiO_2–I complex (Fig. 8). The absence of overlap between the HOMOs of G & J and the conduction band of the TiO_2 cluster is confirmed in the orbitals energies profiles of the complexes as depicted in Fig. 8. Despite not satisfying the requirement of have HOMO levels with the TIO_2 band gap, TiO_2–H complex produce an intermediate occupied level which can enabled ICTT in the visible. This is attributable largely to the strong pie donation from the imidazolium ring to the TiO_2–H coordination. The results revealed that H is similar to N-ethyl-N,N-dimethylpyridin-4-aminium reported by Zhang et al. [36] as an economical and green electrolyte component, which performed dual functions as iodide salt and passive film that suppressed charge recombination. In addition to these dual functions, H is capable ICTT in the visible region, thus, possessing three combination of attributes that are beneficial for simplified DSSC electrolyte recipe and enhanced device performance.

4. Conclusion

We examined adsorption of 4-TBP and its analogues on a model TiO_2 cluster using DFT calculations. Adsorption of 4-TBP on TiO_2 cause a negative of the conduction band edge of TiO_2. Our results showed 4-TBP is capable of ICTT upon adsorption on TiO_2, albeit, in the UV region. When the tertiary butyl group in 4-TBP is replaced with stronger electron donation groups, adsorption of these analogues on TiO_2 produced ICTT in the visible region. No ICTT was indicated when strong electron withdrawing 4-TBP analogue. In contrast, reversed ICTT was implicated for a cationic 4-TBP analogue. Our results showed that para substituted pyridines are capable of ICTT from visible to UV region, no ICTT and even reversed ICTT depending on the nature of the substituted group. Notably, interaction of TiO_2–H complex (H = 4-(1,3,4,5-tetraalkylimidazolium)-2-pyridine), is capable of ICTT in the visible region. H-iodide can served not only as iodide electrolyte, it can also form passive film that can suppress charge recombination. This one component performing three roles will simplified DSSC electrolyte recipe and enhanced device performance. This study revealed there is a broader scope for selection of additives for improving the performance of DSSCs.

CRediT authorship contribution statement

Moyinoluwa O. Ashola: Methodology, Investigation, Data curation. **Richard K. Adeleke:** Software, Formal analysis. **Bolatito E. Olanipekun:** Writing – original draft, Resources, Project administration, Funding acquisition. **Olusola O. James:** Writing – review & editing, Supervision, Conceptualization.

Research data

The research data in this study are orca output files of the DFT calculations. The data files can be supplied on request from the corresponding author.

Declaration of competing interest

We wish to state that there no conflict of interest between the authors.

Acknowledgement

This publication was accomplished by the aid of UNESCO-TWAS Programme, SG-NAPI award financed by German Federal Ministry of Education and Research (Bundesministerium für Bildung und Forschung, BMBF) to B.E Olanipekun (SG-NAPI FR3240330987). The views expressed herein do not necessarily represent those of UNESCO-TWAS or BMBF.

Appendix A. Supplementary data

Supplementary data to this article can be found online at https://doi.org/10.1016/j.jpcs.2025.112558.

Data availability

No data was used for the research described in the article.

References

[1] G. Spinelli, M. Freitag, I. Benesperi, What is necessary to fill the technological gap to design sustainable dye-sensitized solar cells? Sustain. Energy Fuels 7 (2023) 916–927, https://doi.org/10.1039/D2SE01447E.
[2] T.H. Syed, W. Wei, Technoeconomic analysis of dye sensitized solar cells (DSSCs) with WS2/carbon composite as counter electrode material, Inorganics 10 (11) (2022) 191, https://doi.org/10.3390/inorganics10110191.
[3] N.I. Mustafa, N.A. Ludin, N.M. Mohamed, M.A. Ibrahim, M.A.M. Teridi, S. Sepeai, A. Zaharim, K. Sopian, Environmental performance of window-integrated systems using dye-sensitised solar module technology in Malaysia, Sol. Energy 187 (2019) 379–392, https://doi.org/10.1016/j.solener.2019.05.059.
[4] A. Aslam, U. Mehmood, M.H. Arshad, A. Ishfaq, J. Zaheer, A.U.H. Khan, M. Sufyan, Dye-sensitized solar cells (DSSCs) as a potential photovoltaic technology for the self-powered internet of things (IoTs) applications, Sol. Energy 207 (2020) 874–892, https://doi.org/10.1016/j.solener.2020.07.029.
[5] A. Błaszczyk, Strategies to improve the performance of metal-free dye-sensitized solar cells, Dyes Pigments 149 (2018) 707–718, https://doi.org/10.1016/j.dyepig.2017.11.045.
[6] I. Benesperi, H. Michaels, M. Freitag, The researcher's guide to solid-state dye-sensitized solar cells, J. Mater. Chem. C 6 (2018) 11903–11942, https://doi.org/10.1039/C8TC03542C.
[7] J.R. Sofia, K.S. Joseph Wilson, Investigation on short–circuit current density (Jsc) in the dye-sensitized solar cells by optimizing photoelectrode thickness, Optik 290 (2023) 171287, https://doi.org/10.1016/j.ijleo.2023.171287.
[8] S. Rahmana, A. Haleem, M. Siddiq, M.K. Hussain, S. Qamara, S. Hameed, M. Waris, Research on dye sensitized solar cells: recent advancement toward the various constituents of dye sensitized solar cells for efficiency enhancement and future prospects, RSC Adv. 13 (2023) 19508–19529, https://doi.org/10.1039/D3RA00903C.
[9] M. Aftabuzzaman, S. Sarker, C. Lua, H.K. Kim, In-depth understanding of the energy loss and efficiency limit of dye-sensitized solar cells under outdoor and indoor conditions, J. Mater. Chem. A 9 (2021) 24830–24848, https://doi.org/10.1039/D1TA03309C.
[10] K. Sharma, V. Sharma, S.S. Sharma, Dye-sensitized solar cells: fundamentals and current status, Nanoscale Res. Lett. 13 (2018) 381, https://doi.org/10.1186/s11671-018-2760-6.
[11] P.D. Sekaran, R. Marimuthu, An extensive analysis of dye-sensitized solar cell (DSSC), Braz. J. Phys. 54 (2024) 28, https://doi.org/10.1007/s13538-023-01375-w.
[12] Y. Saygili, M. Stojanovic, N. Flores-Díaz, S.M. Zakeeruddin, N. Vlachopoulos, M. Grätzel, A. Hagfeldt, Metal coordination complexes as redox mediators in

regenerative dye-sensitized solar cells, Inorganics 7 (2019) 30, https://doi.org/10.3390/inorganics7030030.
[13] M. Dürr, A. Yasuda, G. Nelles, On the origin of increased open circuit voltage of dye-sensitized solar cells using 4-tert-butyl pyridine as additive to the electrolyte, Appl. Phys. Lett. 89 (2006) 061110, https://doi.org/10.1063/1.2266386.
[14] B.-T. Xiong, B.-X. Zhou, Z.-Y. Zhu, T. Gao, L.-H. Li, J. Cai, W.-M. Cai, Adsorption of 4-tert-Butylpyridine on TiO_2 surface in dye-sensitized solar cells, Chinese J. Chem. 26 (2008) 70–76, https://doi.org/10.1002/cjoc.200890040.
[15] G. Boschloo, A. Hagfeldt, Characteristics of the iodide/triiodide redox mediator in dye-sensitized solar cells, Acc. Chem. Res. 42 (2009) 1819–1826, https://doi.org/10.1021/ar900138m.
[16] M. Göthelid, S. Yu, S. Ahmadi, C. Sun, M. Zuleta, Structure-dependent 4-tert-butyl pyridine-induced band bending at TiO_2 surfaces, Int. J. Photoenergy 2011 (2011) 401356, https://doi.org/10.1155/2011/401356.
[17] J. Wu, Z. Lan, J. Lin, M. Huang, Y. Huang, L. Fan, G. Luo, Electrolytes in dye-sensitized solar cells, Chem. Rev. 115 (2015) 2136–2173, https://doi.org/10.1021/cr400675m.
[18] C. Zhang, J. Dai, Z. Huo, X. Pan, L. Hu, F. Kong, Y. Huang, Y. Sui, X. Fang, K. Wang, S. Dai, Influence of 1-methylbenzimidazole interactions with Li^+ and TiO_2 on the performance of dye-sensitized solar cells, Electrochim. Acta 53 (2008) 5503–5508, https://doi.org/10.1016/j.electacta.2008.03.016.
[19] R. Katoh, M. Kasuya, S. Kodate, A. Furube, N. Fuke, N. Koide, Effects of 4-tert-Butylpyridine and Li ions on photoinduced electron injection efficiency in black-dye-sensitized nanocrystalline TiO2 films, J. Phys. Chem. C 113 (2009) 20738–20744, https://doi.org/10.1021/jp906190a.
[20] J. Fujisawa, S. Kato, M. Hanaya, Adsorption, electronic, and optical properties of TiO_2–pyridine complexes: general principles for interfacial charge-transfer transitions, J. Phys. Chem. C 127 (2023) 17888–17895, https://doi.org/10.1021/acs.jpcc.3c04345.
[21] M. Humayun, F. Raziq, A. Khan, W. Luo, Modification strategies of TiO_2 for potential applications in photocatalysis: a critical review, Green Chem. Lett. Rev. 11 (2) (2018), https://doi.org/10.1080/17518253.2018.1440324.
[22] X. Kang, S. Liu, Z. Dai, Y. He, X. Song, Z. Tan, Titanium dioxide: from engineering to applications, Catalysts 9 (2) (2019) 191, https://doi.org/10.3390/catal9020191.
[23] M. Bledowski, L. Wang, A. Ramakrishnan, O.V. Khavryuchenko, V. D. Khavryuchenko, C. Ricci, J. Strunk, T. Cremer, C. Kolbeck, R. Beranek, Visible-light photocurrent response of TiO_2–polyheptazine hybrids: evidence for interfacial charge-transfer absorption, Phys. Chem. Chem. Phys. 13 (2011) 21511–21519, https://doi.org/10.1039/C1CP22861G.
[24] C. Wu, Q. Fang, Q. Liu, D. Liu, C. Wang, T. Xiang, A. Khalil, S. Chena, L. Song, Engineering interfacial charge-transfer by phase transition realizing enhanced photocatalytic hydrogen evolution activity, Inorg. Chem. Front. 4 (2017) 663–667, https://doi.org/10.1039/C6QI00596A.
[25] N.M. Chauke, R.L. Mohlala, S. Ngqoloda, M.C. Raphulu, Harnessing visible light: enhancing TiO_2 photocatalysis with photosensitizers for sustainable and efficient environmental solutions, Front. Chem. Eng. 6 (2024) 1356021, https://doi.org/10.3389/fceng.2024.1356021.
[26] F. Neese, F. Wennmohs, U. Becker, C. Riplinger, The ORCA quantum chemistry program package, J. Chem. Phys. 152 (2020) 224108, https://doi.org/10.1063/5.0004608.
[27] M.D. Hanwell, D.E. Curtis, D.C. Lonie, T. Vandermeersch, E. Zurek, G.R. Hutchison, Avogadro: an advanced semantic chemical editor, visualization, and analysis platform, J Cheminform 4 (2012) 17, https://doi.org/10.1186/1758-2946-4-17.
[28] N.M. O'Boyle, A.L. Tenderholt, K.M. Langner, Cclib: a library for package-independent computational chemistry algorithms, J. Comput. Chem. 29 (2008) 839–845, https://doi.org/10.1002/jcc.20823.
[29] F. Nunzi, F. De Angelis, Modeling titanium dioxide nanostructures for photocatalysis and photovoltaics, Chem. Sci. 13 (2022) 9485–9497, https://doi.org/10.1039/D2SC02872G.
[30] C.I. Oprea, M.A. Gîrțu, Structure and electronic properties of TiO2 nanoclusters and dye–nanocluster systems appropriate to model hybrid photovoltaic or photocatalytic applications, Nanomaterials 9 (2019) 357, https://doi.org/10.3390/nano9030357.
[31] J. Fujisawa, S. Kato, M. Hanaya, Aromatic-ring dependence of interfacial charge-transfer transitions between TiO_2 nanoparticles and aromatic carboxylic acids, Chem. Phys. Lett. 788 (2022) 139274, https://doi.org/10.1016/j.cplett.2021.139274.
[32] J. Fujisawa, S. Kato, M. Hanaya, Interfacial charge-transfer transitions in weakly coupled TiO_2 complexes with aromatic monothiols for visible-light photocatalytic reactions, J. Phys. Chem. C 126 (2022) 11602–11610, https://doi.org/10.1021/acs.jpcc.2c03521.
[33] J. Fujisawa, M. Nagata, Efficient light-to-current conversion by organic–inorganic interfacial charge-transfer transitions in TiO_2 chemically adsorbed with 2-anthroic acid, Chem. Phys. Lett. 619 (2015) 180–184, https://doi.org/10.1016/j.cplett.2014.11.049.
[34] H. Kusama, H. Orita, H. Sugihara, TiO_2 band shift by nitrogen-containing heterocycles in dye-sensitized solar cells: a periodic density functional theory study, Langmuir 24 (2008) 4411–4419, https://doi.org/10.1021/la703696f.
[35] N.M. Khamaletdinova, A.N. Egorochkin, O.V. Kuznetsova, The binding energy of nitrogen 1s electrons in pyridine derivatives: substituent effects in N-centered radical cations, High Energy Chem. 43 (2009) 427–430, https://doi.org/10.1134/S0018143909060010.
[36] H. Zhang, Y. Shi, L. Wang, C. Wang, H. Zhou, W. Guo, T. Ma, Economical, green and dual-function pyridyl iodides as electrolyte components for high efficiency dye-sensitized solar cells, Chem. Commun. 49 (2013) 9003–9005, https://doi.org/10.1039/C3CC44520H.